PAPER

Bioengineered bile ducts recapitulate key cholangiocyte functions

View the article online for updates and enhancements.

Related content

Biofabrication

PAPER

Bioengineered bile ducts recapitulate key cholangiocyte functions

Chen Chen[1,2] , Paulus G M Jochems[3], Lucia Salz[1], Kerstin Schneeberger[1], Louis C Penning[1], Stan F J van de Graaf[4,5], Ulrich Beuers[4,5], Hans Clevers[2], Niels Geijsen[1,2], Rosalinde Masereeuw [3] and Bart Spee[1]

1   Department of Clinical Sciences of Companion Animals, Faculty of Veterinary Medicine, Utrecht University, The Netherlands
2   Hubrecht Institute-KNAW and University Medical Center Utrecht, Utrecht, The Netherlands
3   Division of Pharmacology, Utrecht Institute for Pharmaceutical Sciences, Faculty of Science, Utrecht University, The Netherlands
4   Tytgat Institute for Liver and Intestinal Research, Academic Medical Center, Amsterdam, The Netherlands
5   Department of Gastroenterology and Hepatology, Academic Medical Center, Amsterdam, The Netherlands

Abstract

Investigation of diseases of the bile duct system and identification of potential therapeutic targets are hampered by the lack of tractable *in vitro* systems to model cholangiocyte biology. Here, we show a step-wise method for the differentiation of murine Lgr5$^+$ liver stem cells (organoids) into cholangiocyte-like cells (CLCs) using a combination of growth factors and extracellular matrix components. Organoid-derived CLCs display key properties of primary cholangiocytes, such as expressing cholangiocyte markers, forming primary cilia, transporting small molecules and responding to farnesoid X receptor agonist. Integration of organoid-derived cholangiocytes with collagen-coated polyethersulfone hollow fiber membranes yielded bioengineered bile ducts that morphologically resembled native bile ducts and possessed polarized bile acid transport activity. As such, we present a novel *in vitro* model for studying and therapeutically modulating cholangiocyte function.

Introduction

Cholangiocytes are the epithelial cells lining the intra- and extra-hepatic biliary tree. The primary physiological function of cholangiocytes is to modify bile and transport bile constituents. The biliary excretion route is important for the elimination of waste products, such as excess cholesterol, bilirubin and hormones, as well as exogenous drugs and toxins from the liver. Cholangiocytes, like hepatocytes, can proliferate to restore damaged bile duct epithelia [1]. Impairment of the regenerative capacity of cholangiocytes can lead to a variety of biliary disorders (cholangiopathies), which together, accounted for approximately 16% of all liver transplants performed in the United States between 1988 and 2014 [2]. While most cholangiopathies in the early stage are restricted to the biliary system, their progression often results in liver cirrhosis and eventually liver failure. While it is relatively easy to culture primary cholangiocytes from multiple species, these cultures are heterogeneous and can only be maintained for 3–4 weeks [3], severely limiting their

application. Moreover, in order to investigate transepithelial transport, cholangiocytes must be cultured as three-dimensional ductular structures, however, *in vitro* models that resemble physiological bile duct epithelia are currently lacking.

To our knowledge, a source of sustainable genetically stable stem cells that can be differentiated into functional cholangiocytes has not been reported. Induced pluripotent stem cells (iPSCs) have been used to generate cholangiocytes *in vitro*, but the generating iPSCs remains low efficient, time-consuming and, in most cases, cells are genetically compromised [4]. In recent years, many internal organs, including the stomach, intestine, liver and pancreas, have been shown to contain adult stem cells that can generate into differentiated cell types of the respective organ. In the liver, the adult stem cells are marked by leucine-rich-repeat-containing G-protein-coupled receptor 5 (Lgr5 is a receptor for the potent Wnt agonists, R-spondins). Lgr5$^+$ cells can be enriched from small pieces of liver tissue and coerced to form organoids, three-dimensional structures recapitulating organ biology, by

creating conditions that mimic the stem cell niche during physiological tissue self-renewal or damage repair [5]. Liver organoids are genetically stable and can be cultured for a prolonged time; both human and murine organoid cultures are able to differentiate towards hepatocytes [6, 7]. Despite this, the use of organoids as a model in cholangiocyte research is limited since key features of mature cholangiocytes, such as bile salt transporter activity, are lost [8].

Here, we report a two-step method to generate cholangiocyte-like cells (CLCs) *in vitro* from murine liver organoids. These organoid-derived CLCs are genetically stable and display essential morphological and functional features of primary cholangiocytes. Furthermore, application of CLCs onto polyethersulfone (PES) hollow fiber membranes (HFM) generate three-dimensional ductal structures that resemble native bile ducts at the structural and functional level. These bioengineered bile ducts offer novel opportunities for studying cholangiocyte biology, modeling cholangiopathies and identification and validation of new therapeutic targets to treat these diseases.

Results

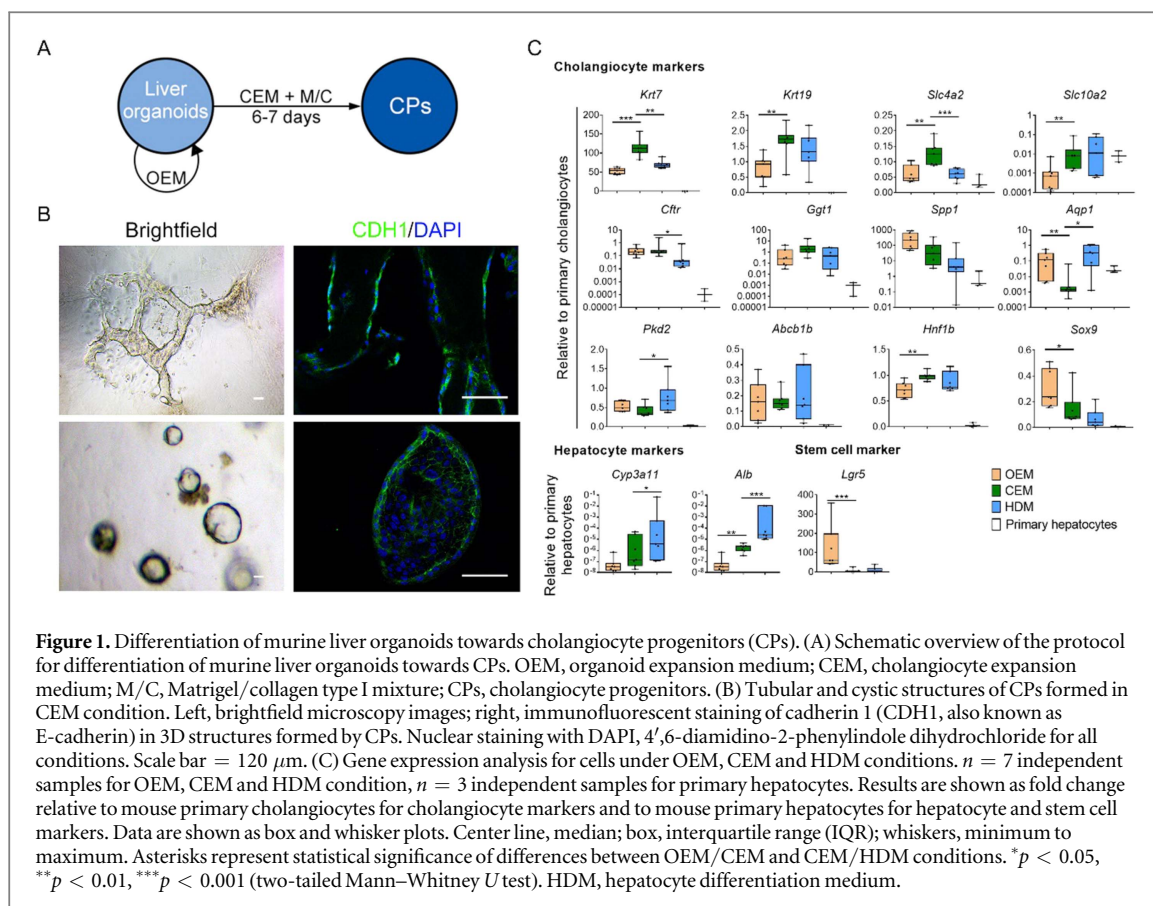### *In vitro* generation of CLCs from murine liver organoids

We based our strategy for the generation of cholangiocytes from liver organoid cultures on established protocols for culture of human primary cholangiocytes [9] and differentiation of hepatic progenitor cells into cholangiocytes [10] (figure 1(A)). Murine liver organoids were expanded from the liver ductal compartment under previously described culture conditions [6]. Subsequently, the organoids were mechanically dissociated into small clusters and suspended in droplets of matrix, consisting of Matrigel and collagen type I. They were maintained in medium designated for biliary lineage differentiation of liver progenitor cells [9]. Under these conditions, Ki67 staining demonstrated that cells preserved their proliferation capacity (figure S1(A) is available online at stacks.iop.org/BF/10/034103/mmedia); therefore, we named this medium cholangiocyte expansion medium (CEM). After 4–6 days in culture, the clusters of cells (hereafter called cholangiocyte progenitors, CPs) grew in size and formed cystic and tubular structures (figure 1(B)). Gene expression analysis (figure 1(C)) demonstrated that CPs displayed increased expression of the following cholangiocyte markers: keratin 7 (*Krt*7), keratin 19 (*Krt*19), HNF1 homeobox B (*Hnf*1b), solute carrier family 10, member 2 (*Slc*10a2, also known as *Asbt*) and solute carrier family 4, member 2 (*Slc*4a2, also known as *Ae*2). Other cholangiocyte markers, ATP-binding cassette, subfamily B, member 1B (*Abcb*1b, also known as *Mdr*1b), polycystic kidney disease 2 (*Pkd*2) and cystic fibrosis

transmembrane conductance regulator (*Cftr*), remained unchanged in CPs and were also expressed in normally expanding liver organoids (OEM). The hepatocyte markers albumin (*Alb*) and cytochrome P450 family 3 subfamily A member 11 (*Cyp*3a11) were expressed in CPs but at significantly lower levels compared to organoid-derived hepatocyte-like cells. In addition, although CPs remained proliferative, the multipotency marker leucine-rich-repeat-containing G-protein-coupled receptor (*Lgr*5) was no longer detectable (figure 1(C)). Taken together, this indicated that the liver organoids differentiated towards the biliary lineage, but still exhibited some immature features.

To promote further maturation of the CPs, we tested small molecule compounds and growth factors including n-acetylcysteine (NAC), gastrin (GAS), taurocholic acid (TCA), fibroblast growth factor 10 (FGF10), and transforming growth factor beta (TGF-β), which have been reported to be directly or indirectly related to biliary functions [11–14]. Of the cholangiocyte markers with low expression in CEM condition, NAC induced aquaporin 1 (*Aqp*1), osteopontin (*Spp*1) and G protein-coupled bile acid receptor 1 (*Gpbar*1) expression, while GAS induced *Spp*1 expression (figure S2). Furthermore, as gene expression analysis showed, the combination of NAC and GAS enhanced the expression of cholangiocyte-enriched transcription factors SRY-box 9 (*Sox*9), one cut domain, family member 1 (*Onecut*1) and one cut domain, family member 2 (*Onecut*2), as well as cholangiocyte markers *Aqp*1, *Gpbar*1 and *Spp*1 in CPs (figures 2(B) and S3). Interestingly, media supplementation with both NAC and GAS reduced the proliferation of CPs as indicated by the quantification of RNA content (figure S4) and Ki67 staining (figure S1(B)). We therefore used this media composition as cholangiocyte differentiation medium (CDM) to drive the CPs towards a more mature CLC phenotype. Immunofluorescence analysis (figures 2(C)–(H)) indicated that epithelial markers, tight junction protein 1 (TJP1, also known as ZO-1) and cadherin 1 (CDH1, also known as E-cadherin), as well as cholangiocyte markers, HNF1B, KRT7, KRT19, AQP1 and gamma-glutamyl transferase 1 (GGT1) were present in CLCs. In contrast, hepatocyte markers, cytochrome P450 family 1 subfamily A member 2 (CYP1A2) and ALB were absent (figures 2(G) and (H)). More importantly, when we stained with acetylated-α-tubulin, we observed that CLCs acquired cilia (figure 2(I)), organelles present in mature cholangiocytes only [15].

Functional characterization of CLCs

Next, we investigated whether the *in vitro*-generated CLCs functionally resembled primary cholangiocytes. In the liver, cholangiocytes are responsible for the reabsorption of bile acids and secretion of small molecules by a series of transmembrane channel

Figure 1. Differentiation of murine liver organoids towards cholangiocyte progenitors (CPs). (A) Schematic overview of the protocol for differentiation of murine liver organoids towards CPs. OEM, organoid expansion medium; CEM, cholangiocyte expansion medium; M/C, Matrigel/collagen type I mixture; CPs, cholangiocyte progenitors. (B) Tubular and cystic structures of CPs formed in CEM condition. Left, brightfield microscopy images; right, immunofluorescent staining of cadherin 1 (CDH1, also known as E-cadherin) in 3D structures formed by CPs. Nuclear staining with DAPI, 4′,6-diamidino-2-phenylindole dihydrochloride for all conditions. Scale bar $= 120$ μm. (C) Gene expression analysis for cells under OEM, CEM and HDM conditions. $n = 7$ independent samples for OEM, CEM and HDM condition, $n = 3$ independent samples for primary hepatocytes. Results are shown as fold change relative to mouse primary cholangiocytes for cholangiocyte markers and to mouse primary hepatocytes for hepatocyte and stem cell markers. Data are shown as box and whisker plots. Center line, median; box, interquartile range (IQR); whiskers, minimum to maximum. Asterisks represent statistical significance of differences between OEM/CEM and CEM/HDM conditions. $^{*}p < 0.05$, $^{**}p < 0.01$, $^{***}p < 0.001$ (two-tailed Mann–Whitney U test). HDM, hepatocyte differentiation medium.
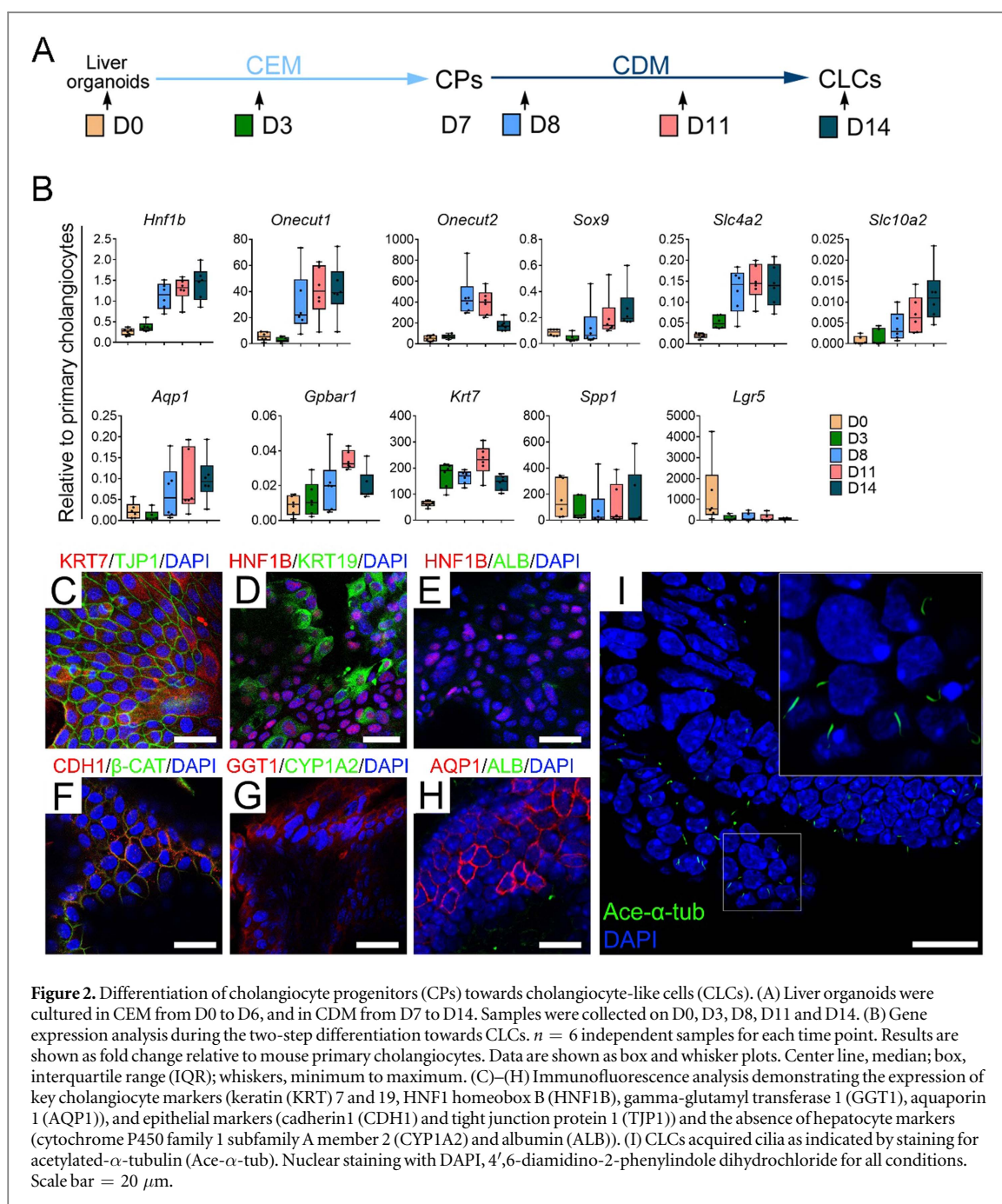
proteins including cystic fibrosis transmembrane conductance regulator (CFTR), apical sodium-dependent bile acid transporter (ASBT, encoded by *Slc10a2*), aquaporin 1 (AQP1), multidrug resistance protein 1B (MDR1B, encoded by *Abcb1b*), and others. To determine the secretory activity of CLCs, we incubated CLCs with Rhodamine 123 (Rh123), a fluorescent chemical compound that can be transported by MDR1B [16]. After incubation, we observed fluorescence accumulation inside both the lumen of the cysts and tubes formed by CLCs (figure 3(A)). This accumulation was blocked when CLCs were treated with the competitive MDR1B inhibitor, Verapamil (figure 3(B)), which confirmed the MDR1B-dependent transport of Rh123.

Several studies have demonstrated the effects of farnesoid X receptor (FXR) signaling in bile acid homeostasis in the liver [17–19]. In cholangiocytes, the activation of FXR signaling leads to the excretion of bile acids, while its inactivation causes intracellular storage of bile acids [20]. To determine this physiological balance in CLCs, we treated them with GW4064, a potent FXR agonist [21]. The expression of *Slc10a2*, which encodes a transporter enhancing the apical surface uptake of bile acids in cholangiocytes, was downregulated (figure 3(C)). In addition, the expression of solute carrier family 51, alpha and beta subunit (*Slc51a* and *Slc51b*; also known as *Ostα* and *Ostβ*), which together form a single transporter responsible for basolateral excretion of bile acids, were significantly up-regulated (figure 3(C)). Together, these results

confirm that the organoid-derived CLCs possess key functionalities of primary cholangiocytes and display an adequate response to external stimuli.

HFM-cultured CLCs forming intact tube-like structures

In vivo, cholangiocytes form a monolayer that lines the lumen of the bile ducts. To investigate whether the organoid-derived CLCs could constitute advanced structures similar to native bile ducts, we used polyethersulfone (PES)HFMs (figures 4(A) and (C)) as the scaffold for culturing CLCs. After two weeks of expansion, HFM-cultured CLCs formed an epithelial barrier, as confirmed by limited inulin-FITC diffusion and the dense arrangement of cells over the HFM (figures 4(B) and (E)). Following another week of CDM culture, gene expression analysis revealed that HFM-cultured CLCs maintained stable expression levels for most cholangiocyte markers (*Hnf1b, Aqp1, Slc10a2, Slc4a2, Cftr,* and *Abcb1b*) compared to CLCs cultured in Matrigel/collagen gel (M/C) alone. Interestingly, cholangiocyte-enriched transcription factors, *Onecut1* and *Onecut2*, and cholangiocyte markers, *Gpbar1* and *Spp1,* were significantly up-regulated in the HFM culture (figure 4(D)). Immunofluorescence analysis also confirmed that HFM-cultured CLCs maintained the expression of cholangiocyte markers (HNF1B, AQP1, GGT1 and KRT7) and epithelial markers (CDH1 and TJP1) (figure 4(E)).
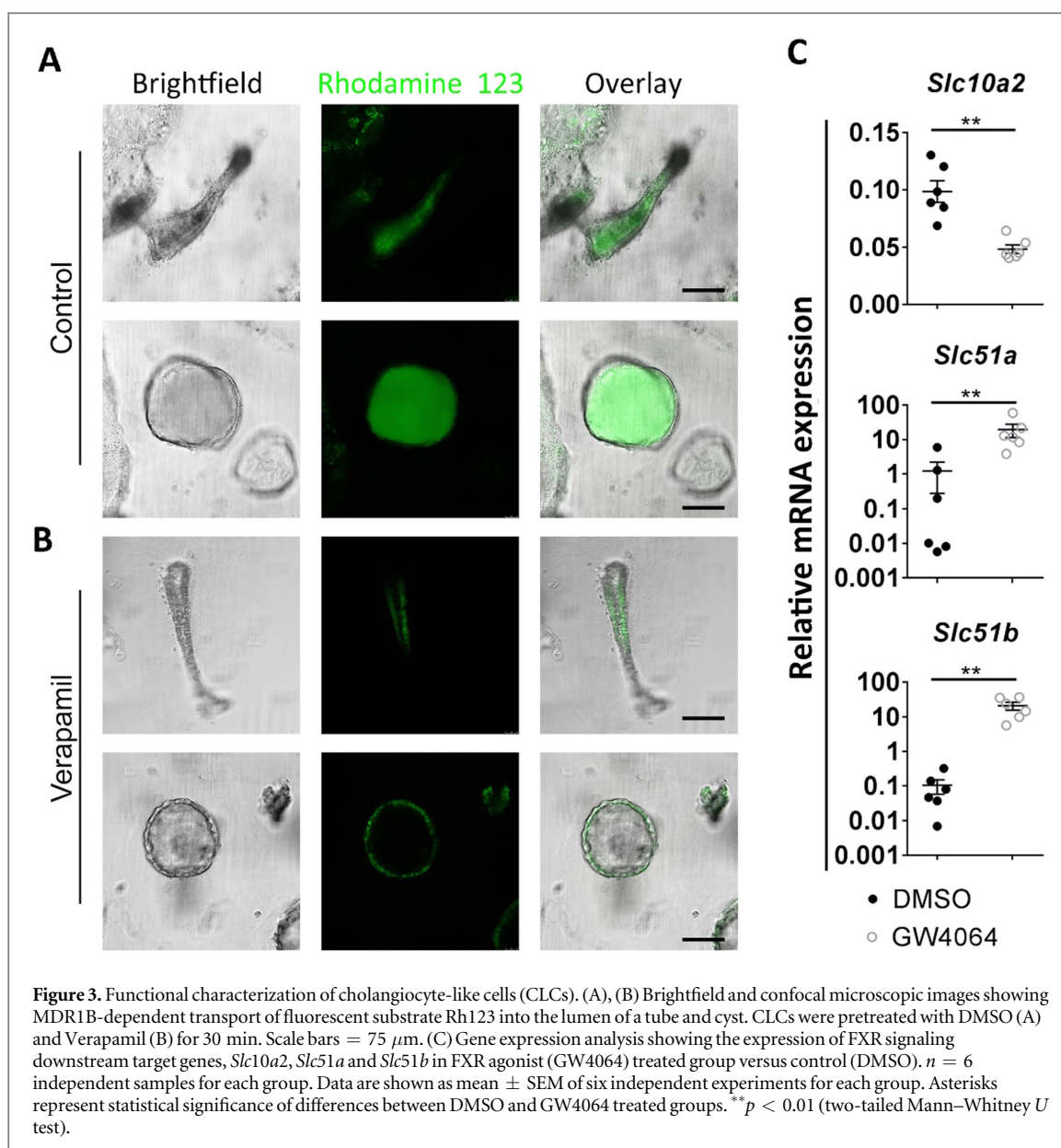
Figure 2. Differentiation of cholangiocyte progenitors (CPs) towards cholangiocyte-like cells (CLCs). (A) Liver organoids were cultured in CEM from D0 to D6, and in CDM from D7 to D14. Samples were collected on D0, D3, D8, D11 and D14. (B) Gene expression analysis during the two-step differentiation towards CLCs. $n = 6$ independent samples for each time point. Results are shown as fold change relative to mouse primary cholangiocytes. Data are shown as box and whisker plots. Center line, median; box, interquartile range (IQR); whiskers, minimum to maximum. (C)–(H) Immunofluorescence analysis demonstrating the expression of key cholangiocyte markers (keratin (KRT) 7 and 19, HNF1 homeobox B (HNF1B), gamma-glutamyl transferase 1 (GGT1), aquaporin 1 (AQP1)), and epithelial markers (cadherin1 (CDH1) and tight junction protein 1 (TJP1)) and the absence of hepatocyte markers (cytochrome P450 family 1 subfamily A member 2 (CYP1A2) and albumin (ALB)). (I) CLCs acquired cilia as indicated by staining for acetylated-α-tubulin (Ace-α-tub). Nuclear staining with DAPI, 4′,6-diamidino-2-phenylindole dihydrochloride for all conditions. Scale bar $= 20$ μm.

Functional characterization of HFM-cultured CLCs

To investigate whether the HFM-cultured CLCs possessed transport activities comparable to native bile ducts, we first determined their cell polarity. Immunofluorescence analysis showed that HFM-cultured CLCs acquired apical-basal polarity. More specifically, the outside of the cell reflected the apical surface (by localization of apical markers, AQP1 and MDR1B), and the inside of the cell reflected the basolateral surface (by localization of the basolateral marker, catenin beta-1 (CTNNB1, also known as β-catenin)); lateral markers (CDH1 and TJP1) were localized in the middle (figures 5(A), (B)). In addition, we observed cilia on the outer surface of HFM-cultured CLCs, as indicated by acetylated-α-tubulin staining (figures 5(C), (D)). This strategy facilitates access to the apical compartment

which can assist transport studies, and also complements M/C culture conditions, where only the basolateral cell surface is accessible.

To measure the transport activity of HFM-cultured CLCs for bile acids, we mounted the HFM into 3D printed bioreactors (figure S5) which had been tested to be non-cytotoxic [22]. *In vivo,* cholangiocytes transport bile acids from the apical surface surrounding the bile duct lumen to the basal surface facing hepatocytes. To study the reabsorption of bile acids from the apical to the basolateral compartment, we applied [^{3}H]taurocholic acid in the bioreactor outside of the HFM-cultured CLCs and determined the radioactivity in the perfusate. As a control for passive diffusion through the epithelium, we measured [^{14}C]inulin, which is not actively transported over cells. We showed that TCA transport

Figure 3. Functional characterization of cholangiocyte-like cells (CLCs). (A), (B) Brightfield and confocal microscopic images showing MDR1B-dependent transport of fluorescent substrate Rh123 into the lumen of a tube and cyst. CLCs were pretreated with DMSO (A) and Verapamil (B) for 30 min. Scale bars = 75 μm. (C) Gene expression analysis showing the expression of FXR signaling downstream target genes, *Slc10a2*, *Slc51a* and *Slc51b* in FXR agonist (GW4064) treated group versus control (DMSO). $n = 6$ independent samples for each group. Data are shown as mean $\pm$ SEM of six independent experiments for each group. Asterisks represent statistical significance of differences between DMSO and GW4064 treated groups. $^{**}p < 0.01$ (two-tailed Mann–Whitney U test).
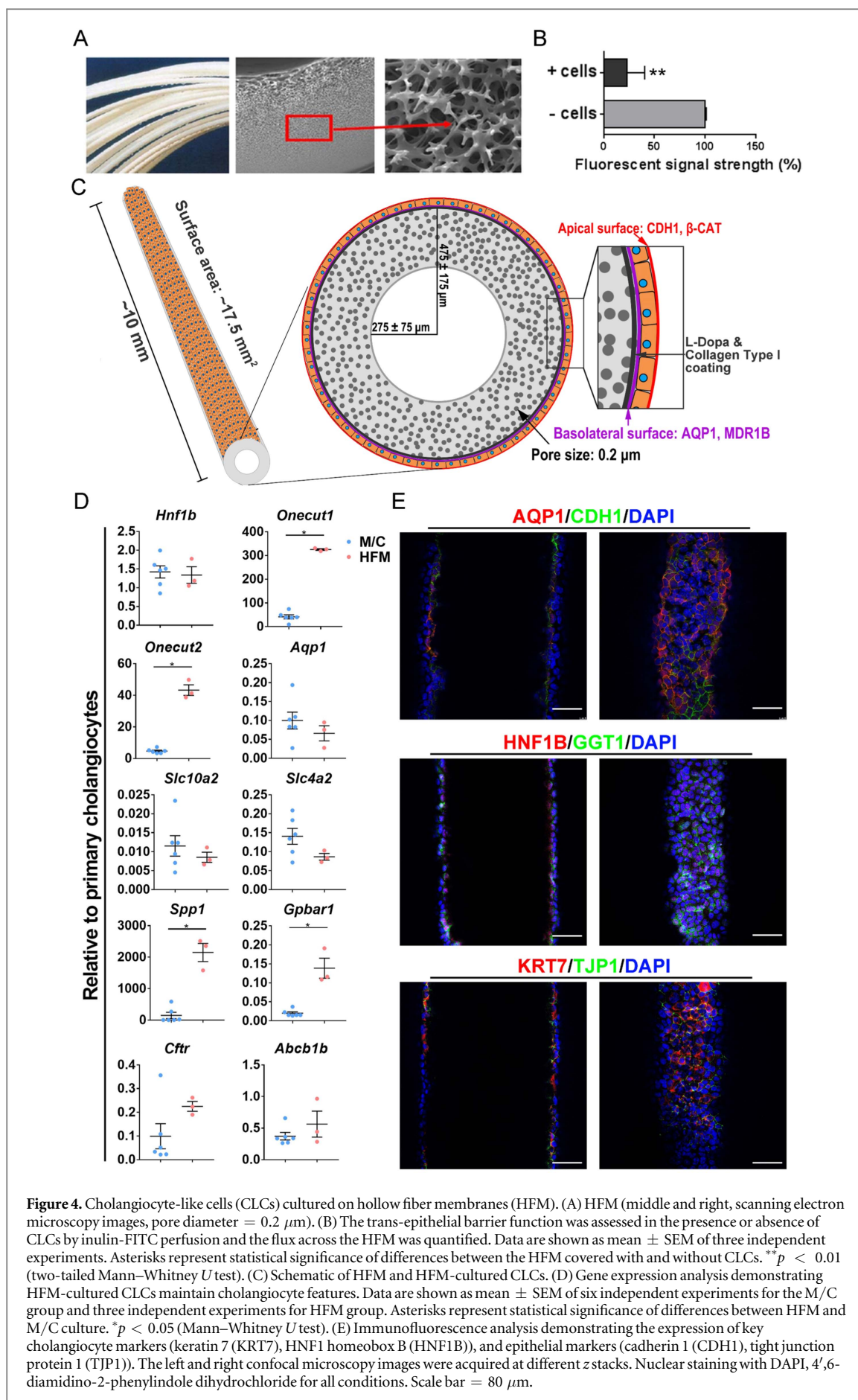
increased rapidly in the first 10 min, then remained relatively stable (figure 5(E)), while inulin diffusion remained at low levels at all time points (figure S6). To further confirm the active transport of TCA, we exposed CLCs to glycochenodeoxycholic acid, which has been shown to inhibit TCA uptake [23]. As figure 5(E) shows, TCA transport was reduced in HFM-cultured CLCs upon treatment with glycochenodeoxycholic acid. Furthermore, we observed accumulation of TCA in carrier-treated HFM-cultured CLCs compared to the glycochenodeoxycholic acid treated CLCs (figure S7). Taken together, these results indicate that HFM-cultured CLCs acquired cell polarity and bile acid transport activity, which is the key function of native bile ducts.
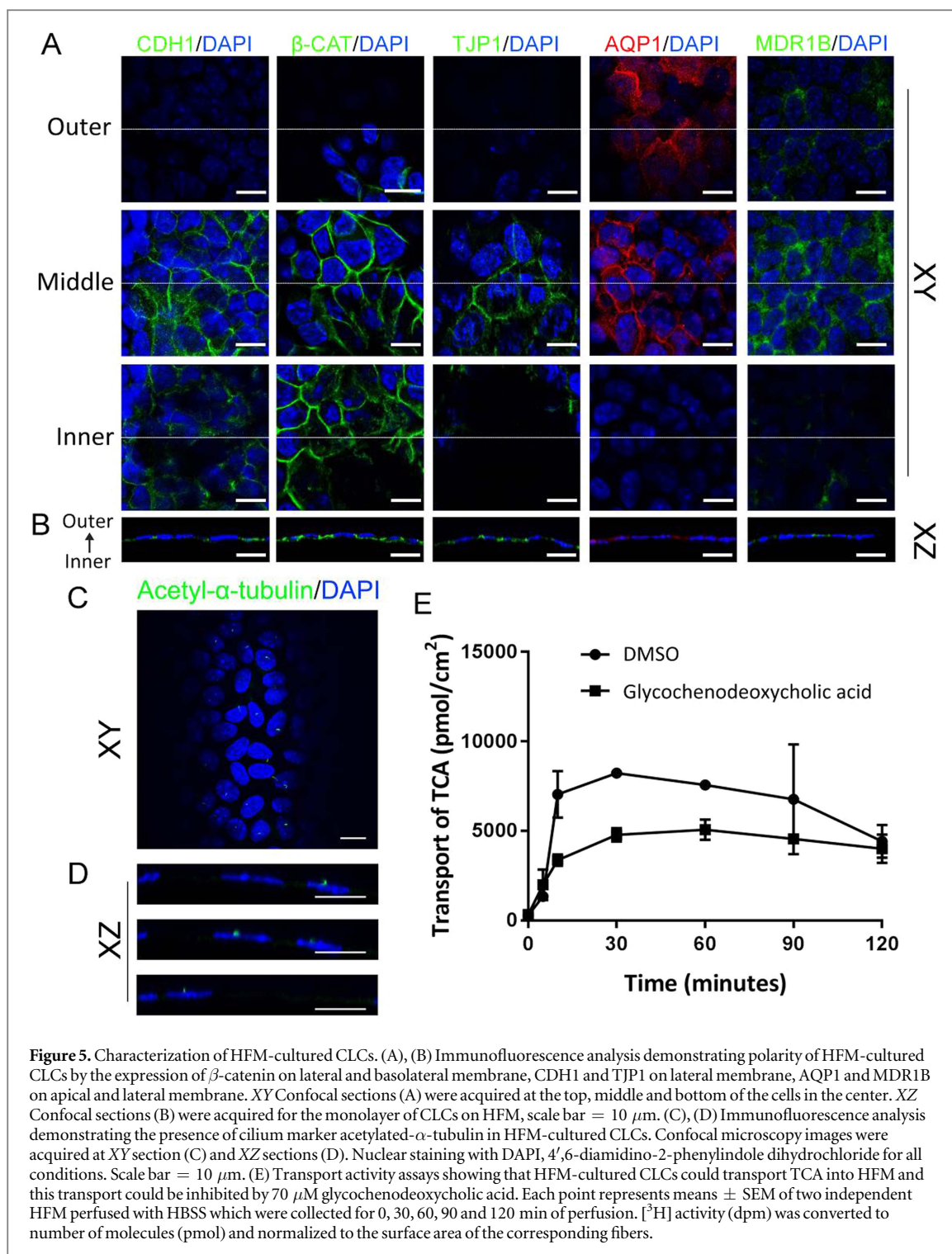
Discussion

Current research and applications of Lgr5^{+} adult liver stem cells, or liver organoids have focused exclusively on their hepatocytic differentiation potential and related hepatic functions [24–26]. This study describes, for the first time, the potential of differentiating liver organoids into mature cholangiocytes. Our results demonstrate that liver organoids are truly bipotent adult stem cells as they can be differentiated towards hepatocytes [6] (figure S8) as well as cholangiocytes.

Functional somatic cells derived from individuals are optimal tools for personalized medicine and disease modeling. This is a valuable advantage over established cell lines, which cannot reflect genetic and potentially epigenetic variation of a broad population. Previous studies have successfully generated cholangiocytes from human iPSCs [27–29], however, generating iPSCs remains low efficient, time-consuming and cells are genetically compromised. Hepatoblasts (the liver stem cells appearing during liver development) have also been proposed for generating cholangiocytes, but this source is difficult to access and

Figure 4. Cholangiocyte-like cells (CLCs) cultured on hollow fiber membranes (HFM). (A) HFM (middle and right, scanning electron microscopy images, pore diameter $= 0.2$ μm). (B) The trans-epithelial barrier function was assessed in the presence or absence of CLCs by inulin-FITC perfusion and the flux across the HFM was quantified. Data are shown as mean $\pm$ SEM of three independent experiments. Asterisks represent statistical significance of differences between the HFM covered with and without CLCs. $^{**}p < 0.01$ (two-tailed Mann–Whitney U test). (C) Schematic of HFM and HFM-cultured CLCs. (D) Gene expression analysis demonstrating HFM-cultured CLCs maintain cholangiocyte features. Data are shown as mean $\pm$ SEM of six independent experiments for the M/C group and three independent experiments for HFM group. Asterisks represent statistical significance of differences between HFM and M/C culture. $^{*}p < 0.05$ (Mann–Whitney U test). (E) Immunofluorescence analysis demonstrating the expression of key cholangiocyte markers (keratin 7 (KRT7), HNF1 homeobox B (HNF1B)), and epithelial markers (cadherin 1 (CDH1), tight junction protein 1 (TJP1)). The left and right confocal microscopy images were acquired at different z stacks. Nuclear staining with DAPI, 4′,6-diamidino-2-phenylindole dihydrochloride for all conditions. Scale bar $= 80$ μm.

Figure 5. Characterization of HFM-cultured CLCs. (A), (B) Immunofluorescence analysis demonstrating polarity of HFM-cultured CLCs by the expression of β-catenin on lateral and basolateral membrane, CDH1 and TJP1 on lateral membrane, AQP1 and MDR1B on apical and lateral membrane. *XY* Confocal sections (A) were acquired at the top, middle and bottom of the cells in the center. *XZ* Confocal sections (B) were acquired for the monolayer of CLCs on HFM, scale bar $= 10$ μm. (C), (D) Immunofluorescence analysis demonstrating the presence of cilium marker acetylated-α-tubulin in HFM-cultured CLCs. Confocal microscopy images were acquired at *XY* section (C) and *XZ* sections (D). Nuclear staining with DAPI, 4′,6-diamidino-2-phenylindole dihydrochloride for all conditions. Scale bar $= 10$ μm. (E) Transport activity assays showing that HFM-cultured CLCs could transport TCA into HFM and this transport could be inhibited by 70 μM glycochenodeoxycholic acid. Each point represents means $\pm$ SEM of two independent HFM perfused with HBSS which were collected for 0, 30, 60, 90 and 120 min of perfusion. [³H] activity (dpm) was converted to number of molecules (pmol) and normalized to the surface area of the corresponding fibers.

important functional tests were lacking in the previous study [10]. Here, we present an alternative approach based on liver organoids. Organoids possess strong *in vitro* proliferation capacity which is mediated by the activation of Wnt signaling by R-spondins [6, 25]. To our surprise, when organoids were exposed to CEM, which is free of Wnt activators, cholangiocyte progenitors continued proliferating for at least four passages.

To drive further maturation of CPs after CEM conditions, we tested a set of small molecule compounds and growth factors and found that a combination of gastrin and n-acetylcysteine optimally drives CP maturation toward CLCs. TGF-β has been reported to be one of the key factors controlling liver stem cells' differentiation and tubulogenesis [11, 14], however, very small amounts of TGF-β (1 ng ml^{-1}) in the medium was fatal for organoids; we therefore excluded it in further studies. It is worth noting that the Growth Factor Reduced Matrigel® used in this study contains approximately 1.7 ng ml^{-1} TGF-β, which may be sufficient for morphogenesis of cholangiocytes. In the liver, cholangiocytes are exposed to

bile. Although it has been demonstrated that tauro-cholic acid, one of the predominant bile acids in human, mice and rats, can induce the differentiation of primary cholangiocytes [13], it did not have an obvious differentiating effect on our CPs (figure S2).

Previous studies showed that gastrin, n-acetylcysteine and FGF10, necessary components in the organoid expansion medium, are also related to cholangiocyte proliferation and function [12, 30, 31]. When CEM was supplemented with gastrin and n-acetylcysteine, the expression of *Aqp*1 was restored and *Gpbar*1 was induced, indicating further maturation of CPs. This may be a consequence of up-regulated expression of cholangiocyte-enriched transcription factors such as *Onecut*1, *Onecut*2 and *Sox*9, which together with *Hnf*1b play central roles on the regulatory network of biliary development [14, 31, 32].

In vivo, cholangiocytes form bile ducts which possess two-way transport activity, for instance, basolateral to apical transport mediated by MDR1 for broad substrate specificity (Rhodamine 123 in our study), and apical to basolateral transport mediated by ASBT or SLC10A2 for bile acids. However, in the Matrigel/collagen type I culture system, the apical membrane of CLCs is inaccessible, which makes the testing of apical-to-basolateral transport technically challenging. Therefore, we introduced the polyethersulfone HFM into the culturing system. The selection of HFM was made because of its hemo-compatible and biocompatible properties, allowing future clinical applications. Although this membrane was designed for low cell adhesion, the membranes appeared well suitable for bioartificial kidney tubules development after coating the membranes with extracellular matrix components. In previous research [33], we biofunctionalized the membrane using a self-polymerizing 3,4-dihydroxy-L-phenylalanine (L-DOPA) which can covalently bind collagen IV [34, 35], an endogenous component in kidney basal lamina that promotes cell differentiation towards epithelial lineages [36, 37]. This coating allowed selective active transport by the renal epithelial barrier and avoided loss of vital blood components when potentially used as renal replacement therapy [22, 33]. By growing cells on the outside of the membrane and applying it in a well-designed perfusion chamber compatible with microscopy, the bioengineered bile ducts can be monitored by confocal imaging allowing functional assessment [22].

In this study, using HFM coated with L-DOPA and collagen I, CLCs organized into polarized epithelial monolayers, where the apical-basolateral polarity is opposite to native bile ducts. Despite this inverted polarity, bioengineered bile ducts can still have a wide range of applications, since both apical and basolateral membrane are exposed to the external environment. Current *in vitro* models for transport studies are cell lines, such as Caco2 and (transfected) MDCK, cultured in dishes or Transwell® systems. These immortalized cells and static cultures poorly mimic the physiological situation, and could fail to predict transporter mediated changes in drug absorption/distribution [38]. The HFM-cultured CLCs can serve as bioengineered bile ducts representing a novel *in vitro* model for drug development, not only because the cells express a variety of channels and pumps, but also the ability to provide dynamic microenvironment for cells. Specifically, the HFM-cultured CLCs can be a model for intrahepatic bile ducts, since they can transport taurocholic acids, which is the key feature of intrahepatic bile ducts [39]. The opposite polarity of the bioengineered bile ducts may even be beneficial to applications in, for instance, bioartificial liver (BAL) devices. Current BAL devices are perfused bioreactors containing only hepatocytes (or hepatocyte-like cells) [40, 41], in which metabolic waste is accumulated overtime. Combining our bioengineered bile ducts with BAL could acquire self-clearance capacity, which would extend the service life of each device, and hence reduce the financial burden (each device needs 3×10^9 cells) [41].

Our current study demonstrates that murine liver organoids are bipotential and can be differentiated into functional hepatocytes and cholangiocytes. By applying them to HFM, these CLCs polarized and possessed key cholangiocyte functions. Although there are intrinsic differences between cholangiocytes between species and even locations within the liver [1], the technology developed here may be applied to human liver organoids, and hence contribute to a better understanding of pathogenetic and therapeutic aspects of cholangiopathies.

Methods

Animals

Surplus liver and gallbladder samples were obtained postmortem from 8 mice that were used in non-liver-related research (experiments approved by the Utrecht University's ethical committee); no animals were harmed or killed for this study.

Culture of murine liver organoids

Murine liver organoids were isolated and cultured as previously described [6]. Briefly, isolated ducts were mixed with Matrigel (BD Biosciences) and seeded. After gelatinization of the Matrigel, culture medium was added. The culture medium (organoids expansion medium, OEM) was based on AdvDMEM/F12 (Invitrogen) supplemented with 1% v/v B27 (Invitrogen), 1% v/v N2 (Invitrogen), 1.25 mM n-acetylcysteine (Sigma-Aldrich), 10 nM gastrin (Sigma-Aldrich), 50 ng ml^{-1} mouse EGF (Invitrogen), 5% v/v R-spondin-1-conditioned medium (the Rspo1-Fc-expressing cell line was a kind gift from Calvin J. Kuo), 100 ng ml^{-1} FGF10 (PeproTech), 10 mM nicotinamide (Sigma-Aldrich), 50 ng ml^{-1} HGF (Pepro-Tech) and 1% v/v Penicillin/Streptomycin (Invitrogen).

Organoids were split by removal from Matrigel using cold AdvDMEM/F12, mechanical dissociation into smaller fragments, and transfer into fresh Matrigel. Passage was performed weekly at a 1:4–1:8 split ratio. The medium was changed every other day.

Differentiation of murine liver organoids to CLCs

Organoids were split by removal from Matrigel using cold DMEM/F12, mechanical dissociation into smaller fragments, and transferred into mixture of Matrigel and 1.2 mg ml^{-1} rat-tail type I collagen at the ratio of 2:3. After 2 h of incubation at 37 °C and, when the gel mixture was solidified, CEM was added. CEM was refreshed every second day. CEM was based on DMEM/F12 supplemented with 10% v/v fetal bovine serum, 1% v/v GlutaMAX (Invitrogen), 1% v/v Non-essential amino acids (Invitrogen), 50 ng ml^{-1} EGF, 50 ng ml^{-1} HGF, 0.1 μM dexamethasone and 1% Penicillin/Streptomycin. After 6 days of CEM culture, the medium was changed to CDM. CDM was based on CEM supplemented with 1.25 mM n-acetylcysteine and 10 nM gastrin. In this medium, cells were cultured for one week. CDM was refreshed every other day.

RNA isolation, cDNA synthesis and RT-qPCR

RNA was isolated from liver organoids, organoid-derived hepatocyte-like cells, M/C- and HFM-cultured CLCs using RNeasy lysis buffer directly added into the plate followed by RNA extraction according to the manufacturer's instructions (Qiagen). cDNA was obtained using the iScript™ cDNA synthesis kit as described by the manufacturer (Bio-Rad, Veenendaal, the Netherlands). A mix of random hexamers and oligo-dT primers were used. Relative gene expression of the selected genes was measured using RT-qPCR. Primer design, validation, RT-qPCR conditions, and data analysis was performed as previously described [42]. Normalization was performed using the reference genes Hypoxanthine phosphoribosyltransferase (*Hprt*) and Hydroxymethylbilane synthase (*Hmbs*). Details of all primers are listed in table S1.

Cholangiocyte functional studies

For the Rhodamine123 (Rh123) transport test, cold DMEM/F12 was used to remove Matrigel and collagen from CLCs. CLCs were pretreated with DMSO or 10 μM Verapamil (Sigma-Aldrich) for 30 min, followed by 5 min of incubation with 100 μM Rh123 (Sigma-Aldrich). Then CLCs were washed 3 times with CDM. Fluorescence (excitation wavelength: 511 nm; emission wavelength: 534 nm) was visualized by Leica SPE-II confocal system after 30 min.

For the FXR activity test, CLCs were incubated in CDM supplemented with 10 μM GW4064 (Sigma-Aldrich) for 48 h and RNA was isolated to determine the expression of downstream signaling of FXR target genes.

Culture of CLCs on double coated HFM

Murine liver organoids were removed from Matrigel using cold AdvDMEM/F12, trypsinized into single cells and small fragments and seeded in culture flasks pre-coated with rat-tail type I collagen. Cells were cultured with CEM. When cells reached confluence, they were trypsinized into single cells and seeded on HFM at a concentration of 1 $\times$ 10^6 cells/4.5 cm fiber. The polyethersulfone HFM (SENUO Filtration Technology Co, Ltd; inner diameter: 550 $\pm$ 150 μm; outer diameter: 950 $\pm$ 350 μm; pore size: 0.2 μm) were prepared using a double coating procedure previously described [33]. Briefly, sterilized fibers were horizontally placed in 1.5 ml Eppendorf tubes and incubated with L-DOPA solution (2 mg ml^{-1} L-3,4-dihydroxy-phenylalanine, 10 mM Tris buffer, pH 8.5) at 37 °C for 4 h, during which fibers were turned 90° every hour. Similarly, the L-DOPA coated fibers were exposed to the rat-tail type I collagen solution (25 μg ml^{-1}) at 37 °C for 2 h, during which fibers were turned 90° every 30 min. The collagen solution was then aspirated and the fibers were washed thoroughly in PBS prior to cell seeding. HFM-cultured cells were placed in 6-well plates and cultured in CEM for 2 weeks for expansion and CDM for 1 week for maturation.

Immunofluorescence analysis

Liver organoids, organoid-derived hepatocyte-like cells, M/C- and HFM-cultured CLCs were fixed in 4% PFA for 30 min and permeabilized with PBS 0.3% Triton X-100 for 30 min. Primary antibodies were incubated overnight. Secondary antibodies were incubated at room temperature for two hours. Tissues were then processed in a click reaction with 5 μM Alexa Fluor® 488 or 568 (Life Technologies) according to manufacturer's instructions. Nuclei were stained with DAPI (Sigma-Aldrich). Tissues were mounted on slides with ProLong® Diamond Antifade Mounting Medium (Invitrogen). Images were acquired using Leica SPE-II confocal system. Antibody details for each protein are shown in table S2.

Trans-epithelial barrier function

Trans-epithelial barrier function was determined as previously described [22]. Briefly, HFM with or without CLCs were connected to a separated in- and outlet glass cannula assembled in a custom-made 3D printed cytocompatible polyester device. HFM were perfused (6 ml h^{-1}) with inulin-fluorescein isothiocyanate (FITC) (0.1 mg ml^{-1} in Krebs–Henseleit buffer) for 10 min at room temperature. 100 μl sample was collected from the outer HFM compartment and its fluorescent strength was measured by a fluorometer (Labsystems).

Bile acid transport assay

HFM with CLCs were connected to a separated in- and outlet glass cannula (inner diameter 120–150 μm;

DMT Trading, Aarhus, Denmark) assembled in a custom-made 3D printed cytocompatible polyester device [22] (figure S5) to enable a separated basolateral (inner HFM, perfusion channel) and apical compartment (outer HFM). The inlet cannula was connected to a tubing system and syringe pump, whereas the outlet cannula was connected to a tubing system and a depot to collect perfusate. During the experiment, 300 μl CDM with [^{14}C]inulin and [^{3}H]taurocholic acid (PerkinElmer) was added to the outer HFM compartment. In the inhibition group, 70 μM glycochenodeoxycholic acids were applied to the outer HFM compartment. Hank's balanced salt solution was perfused (2 ml h^{-1}) through the inner HFM for 2 h at 37 °C. The perfusate was collected at multiple time points. For each time point, 100 μl perfusate was added into 4.9 ml scintillation fluid. Radioactivity was measured by a liquid scintillation counter (Beckman Coulter). Each count was normalized to the surface area of its corresponding HFM.

Statistical analysis

Statistical analysis and graphs were performed using GraphPad Prism 7.0 (GraphPad Software Inc., USA). Data are present as box and whisker plots (minimum to maximum, figures 1(C) and 2(B)) and the mean ± standard error of the mean (figures 3(C) and 4(C)). See figure legends for details on specific statistical tests run and p values calculated for each experiment.

Data availability

All data supporting the finding of this study are included within the paper and its supplementary information.

Acknowledgments

Author contributions

CC, RM and BS conceived the project and designed the experiments; CC, PJ, SG and LS performed the experiments; HC, KS and UB provided resources and helped write the manuscript; CC, LP, NG and BS wrote the paper; all authors were involved in data analysis, discussion and approved the manuscript.

Competing interests

The authors declare no competing financial interests.

ORCID iDs

Chen Chen https://orcid.org/0000-0002-5817-5693
Rosalinde Masereeuw https://orcid.org/0000-0002-1560-1074

References

[1] Tabibian J H, Masyuk A I, Masyuk T V, O'Hara S P and LaRusso N F 2013 Physiology of cholangiocytes *Comprehensive Physiol.* **3** 541–65
[2] Lazaridis K N and LaRusso N F 2015 The cholangiopathies *Mayo Clin. Proc.* **90** 791–800
[3] Joplin R 1994 Isolation and culture of biliary epithelial cells *Gut* **35** 875–8
[4] Sampaziotis F *et al* 2017 Directed differentiation of human induced pluripotent stem cells into functional cholangiocyte-like cells *Nat. Protocols* **12** 814–27
[5] Clevers H 2016 Modeling development and disease with organoids *Cell* **165** 1586–97
[6] Huch M *et al* 2013 *In vitro* expansion of single Lgr5^{+} liver stem cells induced by Wnt-driven regeneration *Nature* **494** 247–50
[7] Huch M *et al* 2015 Long-term culture of genome-stable bipotent stem cells from adult human liver *Cell* **160** 299–312
[8] Alpini G *et al* 2005 Secretin activation of the apical Na^{+}-dependent bile acid transporter is associated with cholehepatic shunting in rats *Hepatology* **41** 1037–45
[9] Tanimizu N *et al* 2013 Hepatic biliary epithelial cells acquire epithelial integrity but lose plasticity to differentiate into hepatocytes *in vitro* during development *J. Cell Sci.* **126** 5239–46
[10] Tanimizu N, Miyajima A and Mostov K E 2007 Liver progenitor cells develop cholangiocyte-type epithelial polarity in three-dimensional culture *Mol. Biol. Cell* **18** 1472–9
[11] Antoniou A *et al* 2009 Intrahepatic bile ducts develop according to a new mode of tubulogenesis regulated by the transcription factor SOX9 *Gastroenterology* **136** 2325–33
[12] Glaser S *et al* 2003 Gastrin reverses established cholangiocyte proliferation and enhanced secretin-stimulated ductal secretion of BDL rats by activation of apoptosis through increased expression of Ca^{2+}-dependent PKC isoforms *Liver Int.* **23** 78–88
[13] Alpini G *et al* 2001 Bile acid feeding increased proliferative activity and apical bile acid transporter expression in both small and large rat cholangiocytes *Hepatology* **34** 868–76
[14] Clotman F *et al* 2005 Control of liver cell fate decision by a gradient of TGFβ signaling modulated by onecut transcription factors *Genes Dev.* **19** 1849–54
[15] Huang B Q *et al* 2006 Isolation and characterization of cholangiocyte primary cilia *Am. J. Physiol. Gastrointest. Liver Physiol.* **291** 500–9
[16] Tang F, Ouyang H, Yang J Z and Borchardt R T 2004 Bidirectional transport of rhodamine 123 and hoechst 33342, fluorescence probes of the binding sites on P-glycoprotein, across MDCK-MDR1 cell monolayers *J. Pharm. Sci.* **93** 1185–94
[17] Li G and Guo G L 2015 Farnesoid X receptor, the bile acid sensing nuclear receptor, in liver regeneration *Acta Pharm. Sin. B* **5** 93–8
[18] Ding L, Yang L, Wang Z and Huang W 2015 Bile acid nuclear receptor FXR and digestive system diseases *Acta Pharm. Sin. B* **5** 135–44
[19] Chiang J 2013 Bile acid metabolism and signalling *Comprehensive Physiol.* **3** 1191–212

[20] Jones H, Alpini G and Francis H 2015 Bile acid signaling and biliary functions *Acta Pharm. Sin.* B **5** 123–8

[21] Maloney P R *et al* 2000 Identification of a chemical tool for the orphan nuclear receptor FXR *J. Med. Chem.* **43** 2971–4

[22] Jansen J *et al* 2015 Human proximal tubule epithelial cells cultured on hollow fibers: living membranes that actively transport organic cations *Sci. Rep.* **5** 16702

[23] Balakrishnan A, Sussman D J and Polli J E 2005 Development of stably transfected monolayer overexpressing the human apical sodium-dependent bile acid transporter (hASBT) *Pharm. Res.* **22** 1269–80

[24] Kruitwagen H S *et al* 2017 Long-term adult feline liver organoid cultures for disease modeling of hepatic steatosis *Stem Cell Rep.* **8** 822–30

[25] Nantasanti S *et al* 2015 Disease modeling and gene therapy of copper storage disease in canine hepatic organoids *Stem Cell Rep.* **5** 895–907

[26] Huch M, Boj S F and Clevers H 2013 Lgr5(+) liver stem cells, hepatic organoids and regenerative medicine *Regen. Med.* **8** 385–7

[27] Sampaziotis F *et al* 2015 Cholangiocytes derived from human induced pluripotent stem cells for disease modeling and drug validation *Nat. Biotechnol.* **33** 845–52

[28] Dianat N *et al* 2014 Generation of functional cholangiocyte-like cells from human pluripotent stem cells and HepaRG cells *Hepatology* **60** 700–14

[29] Ogawa M *et al* 2015 Directed differentiation of cholangiocytes from human pluripotent stem cells *Nat. Biotechnol.* **33** 853–61

[30] Zhang W *et al* 2007 Aquaporin-1 channel function is positively regulated by protein kinase C *J. Biol. Chem.* **282** 20933–40

[31] Si-Tayeb K, Lemaigre F P and Duncan S A 2010 Organogenesis and development of the liver *Dev. Cell* **18** 175–89

[32] Clotman F *et al* 2002 The onecut transcription factor HNF6 is required for normal development of the biliary tract *Development* **129** 1819–28

[33] Schophuizen C M S *et al* 2015 Development of a living membrane comprising a functional human renal proximal tubule cell monolayer on polyethersulfone polymeric membrane *Acta Biomater.* **14** 22–32

[34] Oo Z Y *et al* 2011 The performance of primary human renal cells in hollow fiber bioreactors for bioartificial kidneys *Biomaterials* **32** 8806–15

[35] Lee H, Rho J and Messersmith P B 2009 Facile conjugation of biomolecules onto surfaces via mussel adhesive protein inspired coatings *Adv. Mater.* **21** 431–4

[36] Zhang H, Tasnim F, Ying J Y and Zink D 2009 The impact of extracellular matrix coatings on the performance of human renal cells applied in bioartificial kidneys *Biomaterials* **30** 2899–911

[37] Oliver J A, Barasch J, Yang J, Herzlinger D and Al-Awqati Q 2002 Metanephric mesenchyme contains embryonic renal stem cells *Am. J. Physiol. Physiol.* **283** F799–809

[38] Awortwe C, Fasinu P S and Rosenkranz B 2014 Application of Caco-2 cell line in herb-drug interaction studies: current approaches and challenges *J. Pharm. Pharm. Sci.* **17** 1–19

[39] Cheung A C, Lorenzo Pisarello M J and LaRusso N F 2018 Pathobiology of biliary epithelia *Biochim. Biophys. Acta—Mol. Basis Dis.* **1864** 1220–31

[40] van de Kerkhove M P, Hoekstra R, Chamuleau R A F M and van Gulik T M 2004 Clinical application of bioartificial liver support systems *Ann. Surg.* **240** 216–30

[41] Shi X-L *et al* 2016 Improved survival of porcine acute liver failure by a bioartificial liver device implanted with induced human functional hepatocytes *Cell Res.* **26** 206–16

[42] van Steenbeek F G *et al* 2013 Altered subcellular localization of heat shock protein 90 is associated with impaired expression of the aryl hydrocarbon receptor pathway in dogs *PLoS One* **8** e57973